The intrinsic shape and dynamical structure of the bulges of lenticular galaxies

2014 J. Phys.: Conf. Ser. 566 012009

(http://iopscience.iop.org/1742-6596/566/1/012009)

Journal of Physics: Conference Series **566** (2014) 012009 doi:10.1088/1742-6596/566/1/012009

The intrinsic shape and dynamical structure of the bulges of lenticular galaxies

L Costantin[1], E M Corsini[1,2], J Méndez-Abreu[3], E Dalla Bontà[1,2], L Morelli[1,2] and A Pizzella[1,2]

[1] Dipartimento di Fisica e Astronomia, Università di Padova, Italy
[2] INAF-Osservatorio Astronomico di Padova, Italy
[3] School of Physics and Astronomy, University of St. Andrews, UK

E-mail: luca.costantin@studenti.unipd.it, enricomaria.corsini@unipd.it, jma20@st-andrews.ac.uk, elena.dallabonta@unipd.it, lorenzo.morelli@unipd.it, alessandro.pizzella@unipd.it

Abstract. Several scenarios have been proposed to account for the formation and evolution of galactic bulges and to explain the variety of their observed properties. Both the intrinsic shape and dynamical structure of bulges depend on the mechanisms and timescales of their formation. We are deriving the intrinsic axial ratios of the bulges of a sample of unbarred lenticular galaxies to look for a possible relationship with their known orbital structure. Preliminary results show that the orbits of stars of the triaxial bulge of NGC 4476 are more anisotropic than those in the axisymmetric bulge of NGC 4249 hinting at a different formation process.

1. Introduction

Several formation scenarios were proposed to explain the variety of photometric, kinematic, dynamical, and stellar population properties observed in bulges of lenticular and spiral galaxies. Classical bulges are similar to low-luminosity elliptical galaxies and they are thought to be formed by rapid gravitational collapse or hierarchical merging; boxy/peanut-shaped bulges are bars and formed from dynamical instabilities of the galactic disks; pseudobulges are reminiscent of disks and formed from secular processes of redistribution of the gas and stars driven by bars or environmental effects (see [1], for a review). This picture is further complicated by the co-existence of mixed types of classical and pseudobulges in the same galaxy [2, 3] and their combination with boxy/peanut structures in barred galaxies [4, 5].

Studying the intrinsic shape of the bulges provides a crucial piece of information for testing the results of numerical simulations of bulge formation. About 80% of bulges in unbarred lenticular and early-to-intermediate spiral galaxies are not oblate but triaxial ellipsoids [6] and the distribution of bulge triaxiality is strongly bimodal [7]. According to numerical simulations, bulges with a Sérsic index $n \leq 2$ which show a high fraction of oblate axisymmetric (or nearly axisymmetric) shapes and have a bulge-to-total ratio $B/T \leq 0.3$, may be the result of dissipational minor mergers. Both major dissipational and dissipationless mergers seem to be required to explain the variety of shapes found for bulges with $n > 2$ and $B/T > 0.3$ (e.g., [8]).

We started a project to analyze the structural and dynamical properties of the bulges of a sample of unbarred lenticular galaxies in order to study the relationship between their intrinsic

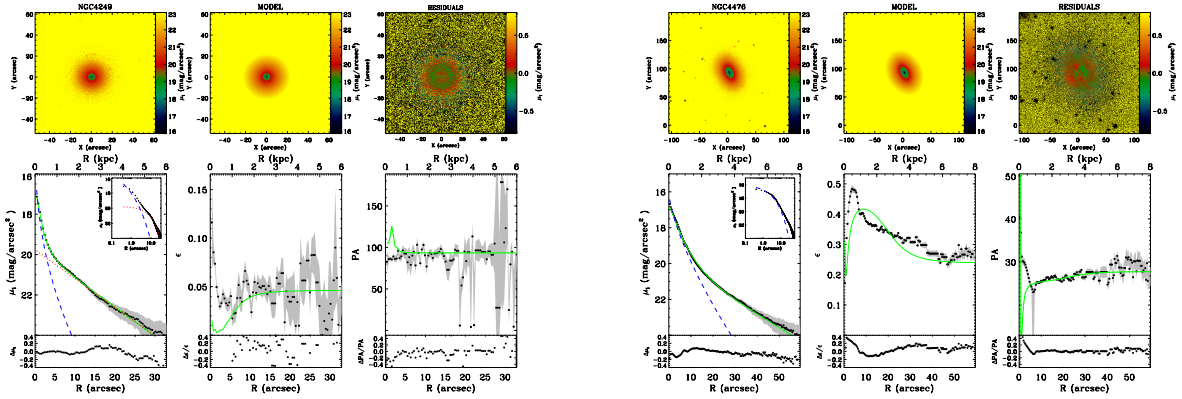

Figure 1. Two-dimensional photometric decomposition of the fast-rotating galaxy NGC 4249 (left plot) and slow-rotating galaxy NGC 4476 (right plot) obtained from GASP2D. Upper panels (from left to right): map of the observed, modeled, and residual (observed−modeled) surface brightness distribution of the galaxy. Lower panels (from left to right): ellipse-averaged radial profile of surface brightness, position angle, and ellipticity measured in the observed (dots with error bars) and modeled image (green solid line). The surface-brightness radial profiles of the fitted bulge (blue dashed line) and disk (red dotted line) are also shown.

shape and orbital structure. In this paper we present the preliminary results for the bulges of the two S0 galaxies NGC 4249 and NGC 4476.

2. Galaxy sample

Our sample comprises 46 objects from the volume-limited ATLAS^{3D} sample of 260 early-type galaxies with a distance $d < 40$ Mpc [9]. The sample galaxies were selected to be classified as SA0 [10]; with inclination $i < 65°$ to successfully perform the photometric decomposition; without morphological (e.g., signatures of interactions; [9]) and/or kinematic (e.g., evidence for decoupled components; [11]) peculiarities; with i-band images in the data archive of the Sloan Digital Sky Survey (SDSS), [12].

3. Photometric parameters of the bulge and disk

The photometric decomposition of the i-band SDSS images of the sample galaxies was performed using the GASP2D algorithm [6], which yields the structural parameters for a Sérsic bulge and an exponential disk.

The fitting algorithm relies on a χ^2 minimization of the intensities in counts, for which we must adopt initial trial parameters that are as close as possible to their final values. The trial values of the effective surface brightness, effective radius, shape parameter, position angle, and axial ratio of the bulge (I_e, r_e, n, PA_b, and q_b) and of the central surface brightness, scale-length, position angle, and axial ratio of the disk (I_0, h, PA_d, and q_d) were estimated from the analysis of the ellipse-averaged radial profiles of surface brightness μ_i, ellipticity ϵ, and position angle PA. The latter were measured using the IRAF task ELLIPSE [13]. Starting from these initial trial parameters the different photometric models of the surface brightness were fitted iteratively to the galaxy image. Each image pixel was weighted according to the variance of its total observed photon counts due to the contribution of both galaxy and sky, and determined assuming photon noise limitation and taking the detector read-out noise into account. Seeing effects were also

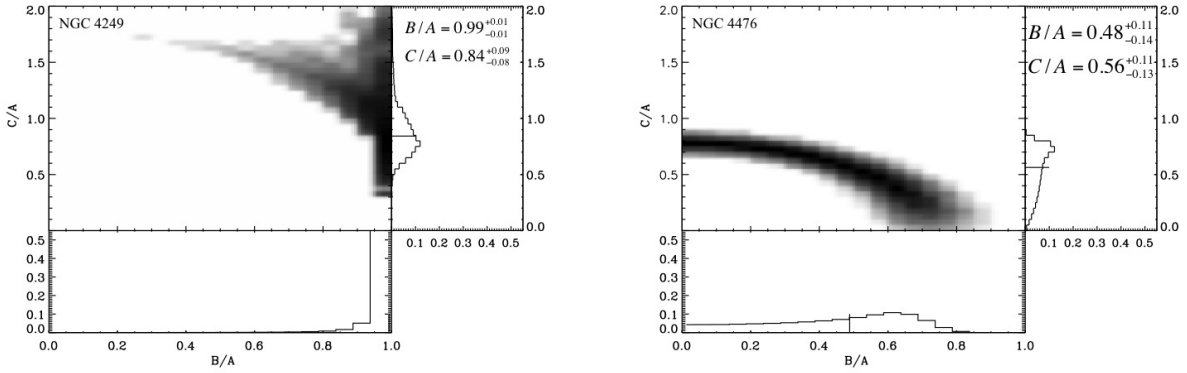

Figure 2. The distribution of the intrinsic axial ratios of the bulge of NGC 4249 (left plot) and NGC 4476 (right plot). For each galaxy, the median value of B/A and C/A is given and marked with a segment in the bottom and right panel, respectively.

taken into account by convolving the model image with a circular Moffat point spread function (PSF) with a FWHM matching the observed one. The convolution was performed as a product in Fourier domain before the least-squares minimization. Only the image pixels with an intensity larger than the sky standard deviation were included in the fit. Foreground stars were masked and excluded from the fit.

The analysis of the fitted images allowed to reject 29 galaxies since they either turned out to be ellipticals or showed a bar and/or spiral arms. The result of the photometric decomposition of the images of NGC 4249 and NGC 4476 is shown in figure 1.

The errors on the fitted parameters were estimated through Monte Carlo simulations on images of artificial galaxies. Finally, a background level and photon noise were added to the simulated images in order to mimic the instrumental setup and image signal-to-noise ratio. The relative errors in the fitted parameters of the artificial galaxies were estimated by comparing the input and output values and were assumed to be normally distributed. The standard deviation was adopted as the 1σ error in the relevant parameter for the bulge-disk decomposition. Systematic errors given by a wrong estimation of the PSF FWHM and sky level are the most significant contributors to the error budget. To derive the intrinsic shape of the bulge we are interested in q_b, q_d, $\mathrm{PA_b}$, and $\mathrm{PA_d}$. Their 3σ errors including systematics are smaller than 15%.

4. Intrinsic shape of the bulges

The intrinsic shape of the sample bulges was derived from the geometrical relationships between the projected and intrinsic shapes of the bulge and its surrounding disk (see [7] for details). The bulge is assumed to be a triaxial ellipsoid with semi-axes of length A and B in the equatorial plane and C along the polar axis. The bulge shares the same center and polar axis as the disk, which is circular and lies on the equatorial plane of the bulge. The intrinsic shape of the bulge is recovered from the bulge ellipticity parameter $e = (1 - q_\mathrm{b}^2)/(1 + q_\mathrm{b}^2)$, twist angle $\delta = 180^\circ - |\mathrm{PA_b} - \mathrm{PA_d}|$ between the major axes of the bulge and disk (i.e., the line of nodes), and disk inclination $\theta = \arccos q_\mathrm{d}$.

The relation between the intrinsic and projected parameters depends only on the spatial position of the bulge, i.e., on the angle $0 \leq \phi \leq 90^\circ$ measured on the bulge equatorial plane between the principal axis corresponding to A and the line of nodes. The equatorial ellipticity $Z = B^2/A^2$ and intrinsic flattening $F = C^2/A^2$ of the bulge are given by:

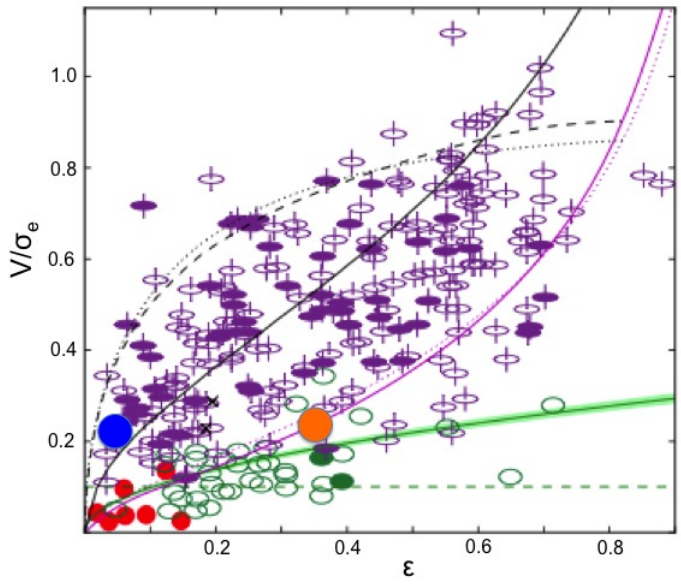

Figure 3. (ϵ, V/σ) diagram of the ATLAS^{3D} galaxies (see [14] for details). NGC 4249 (blue circle) and NGC 4476 (orange circle) are shown together with the non-rotating galaxies (red symbols), non-regular rotators without any specific kinematic feature (green symbols), and regular rotators (purple symbols). The solid black line corresponds to isotropic oblate systems viewed edge-on.

$$\frac{\sin(2\phi_C)\,\sin^2\theta}{\cos^2\theta}F = -\sin\phi_B\cos(2\phi_C-\phi_B)\,(1+Z)^2 + \sin(2\phi_C-\phi_B)\sqrt{(1-Z)^2-\sin^2\phi_B\,(1+Z)^2}\,, \tag{1}$$

where:

$$\phi_B = \arctan\frac{e\,\sin 2\delta}{\cos\theta\,(1+e\,\cos 2\delta)}\,, \tag{2}$$

$$\phi_C = \frac{1}{2}\arctan\frac{2\,e\,\sin 2\delta\,\cos\theta}{e\,\cos 2\delta\,(1+\cos^2\theta)-\sin^2\theta}\,. \tag{3}$$

Since the axial ratios B/A and C/A are both functions of the same variable ϕ, their probabilities are identical, i.e., for a given value of B/A with probability $P(B/A)$, the corresponding value of C/A obtained by equation (1) has a probability $P(C/A) = P(B/A)$. This allows to obtain the range of possible values of B/A and C/A for the bulge and to constrain its most probable intrinsic shape by adopting the probabilities $P(Z)$ and $P(F)$, [7].

The distribution of B/A and C/A for the bulges of NGC 4249 and NGC 4476 as calculated via Monte Carlo simulations is shown in figure 2. We randomly chose 5000 geometric configurations assuming a Gaussian distribution of $q_{\rm b}$, $q_{\rm d}$, $\mathrm{PA_b}$, and $\mathrm{PA_d}$ taking into account their 3σ errors. For each geometric configuration we derived 1000 values of B/A and C/A according to their probability distribution functions. The resulting median values of the axial ratios and the 1σ

confidence intervals from their cumulative distribution are $B/A = 0.99^{+0.01}_{-0.01}$ and $C/A = 0.84^{+0.09}_{-0.08}$ for the bulge of NGC 4249 and $B/A = 0.48^{+0.11}_{-0.14}$ and $C/A = 0.56^{+0.11}_{-0.13}$ for the bulge of NGC 4476, respectively.

5. Conclusions

The two S0 galaxies NGC 4249 and NGC 4476 are classified as a fast and slow rotator, respectively (figure 3, [14]). Slow rotators exhibit complex stellar velocity fields and often include stellar kinematically distinct cores, fast rotators have regular velocity fields and show aligned photometric and kinematic axes.

We have found that the bulge of NGC 4249 is axisymmetric and almost spherical, whereas the bulge of NGC 4476 is triaxial and partially prolate (figure 2). From the location of NGC 4249 and NGC 4476 in the (ϵ, V/σ) diagram (figure 3), we conclude that the orbits of stars of the triaxial bulge of NGC 4476 are more anisotropic than those in the axisymmetric bulge of NGC 4249.

This is in agreement with the recent findings on the shape of the ATLAS^{3D} early-type galaxies [15]. It has been shown that the fast rotators are predominantly axisymmetric, whereas slow rotators are mildly triaxial hinting at different formation scenarios. However, their photometric and kinematic properties are representative of the galaxy as a whole, and therefore, no attempt to account for the different structural components of the galaxies (i.e., bulge, disk and bar) or even to distinguish elliptical and lenticular galaxies was made. Moreover, a Gaussian intrinsic shape distribution under assumption of axisymmetry has been adopted in the photometric analysis. We plan to address the above issues for the bulges of lenticular galaxies by completing the analysis of their intrinsic shape and orbital structure for all the objects of our sample.

Acknowledgments

This work was supported by Padua University through grants 60A02–5052/11, 60A02–4807/12, 60A02–5857/13, and CPDA133894. J.M.A. acknowledges support from the European Research Council Starting Grant (SEDmorph; P.I. V. Wild). L.M. received financial support from Padua University grant CPS0204. L.C. acknowledges the University of St. Andrews for their hospitality while this paper was in progress.

References

[1] Kormendy J and Kennicutt R C 2004 *ARA&A* **42** 603
[2] Gadotti D A 2009 *MNRAS* **393** 1531
[3] Nowak N, Thomas J, Erwin P, Saglia R P, Bender R and Davies R I 2010 *MNRAS* **403** 646
[4] Athanassoula E 2005 *MNRAS* **358** 1477
[5] Méndez-Abreu J, Debattista V P, Corsini E M and Aguerri J A L 2014 *A&A* in press
[6] Méndez-Abreu J, Aguerri J A L, Corsini E M and Simonneau E 2008 *A&A* **478** 353
[7] Méndez-Abreu J, Simonneau E, Aguerri J A L and Corsini E M 2010 *A&A* **521** A71
[8] Cox T J, Jonsson P, Primack J R and Somerville R S 2006 *MNRAS* **373** 1013
[9] Cappellari M et al. 2011 *MNRAS* **413** 813
[10] de Vaucouleurs G, de Vaucouleurs A, Corwin H G, Jr, Buta R J, Paturel G and Fouqué P 1991 *Third Reference Catalogue of Bright Galaxies* (New York, NY: Springer)
[11] Krajnović D et al. 2011 *MNRAS* **414** 2923
[12] York D G et al. 2000 *AJ* **120** 1579
[13] Jedrzejewski R I 1987 *MNRAS* **226** 747
[14] Emsellem E et al. 2011 *MNRAS* **414** 888
[15] Weijmans A-M et al. 2014 *MNRAS* in press